OPTICALLY MEASURING MILLIKELVIN TEMPERATURE VARIATIONS

Ionuț VLĂDOIU[1], Mihai-Alin FLORICEL[2], Petrișor-Gabriel BLEOTU[3], Adrian RADU[4]

Ultra-small temperature variations measurements are usually not a trivial task. However, we propose an experimental setup which is relatively simple and can be achieved in a university teaching laboratory. The method used in this study combines a laser interferometer and a bimetal as a temperature sensor to accurately measure milliKelvin temperature variations. We used this setup to quantify the heating capability of low-power continuous laser beams.

Keywords: milliKelvin, laser interferometer, bimetal, interference, laser heating.

1. Introduction

Currently, temperature can be measured using various techniques [1-5], including resistance and capacitance thermometers, thermocouples, thermistors, quartz thermometers, magnetic thermometers, pyrometers and infrared detectors, laser-based and optical fiber probes, thermographic phosphors, and thermochromic liquid crystals. Quantitatively evaluating temperatures within $0.2\,\mathrm{K}$ precision is currently used in everyday life, for example in clinical applications [6]. However, precise temperature measurements are not trivial and special techniques must be developed for this purpose. Platinum resistance thermometers were used to define the international temperature scale with the accuracy of $\pm 2\,\mathrm{mK}$ at its lower end and $\pm 7\,\mathrm{mK}$ at its upper end [7]. However, commercially available standard platinum resistance thermometers can achieve the maximum accuracy of $\pm 10\,\mathrm{mK}$ [8]. The accuracy of special thermistor devices can be better then $\pm 10\,\mathrm{mK}$ [9]. Noise thermometers based on the relationship between Nyquist or Johnson noise and thermodynamic temperature have been developed [10-12]. Based on thermal magnetic noise, a type of thermometer that functions between approximately $10\,\mathrm{mK}$ and $4\,\mathrm{K}$ with a precision of a few mK was proposed [13]. However, except at very low

[1] Lect., Dept. of Physics, University POLITEHNICA of Bucharest, Romania
[2] Eng., Interdisciplinary Doctoral School, Transilvania University of Brașov, Romania
[3] Eng., Horia Hulubei National Institute for R&D in Physics and Nuclear Engineering, Romania
[4] Prof., Dept. of Physics, University POLITEHNICA of Bucharest, Romania,
e-mail: adrian.radu@physics.pub.ro

temperatures, the accuracy of noise thermometers does not match that of other simpler instruments such as resistance temperature detectors. Paramagnetic thermometry uses special materials and may reach a reproducibility better than $0.5\ \mathrm{mK}$ below $50\ \mathrm{K}$ with an uncertainty of $1\ \mathrm{mK}$ [14].

In this study, we present a technique for measuring temperature variations based on laser interferometry and dilatation of bimetals. Accurately measuring the absolute temperature on the true Kelvin scale is much more complicated than measuring temperature variations with great accuracy because absolute temperature cross-calibration is very difficult to achieve.

The remainder of this paper is organized as follows. Section 2 presents the idea and theory of the method. Section 3 describes the experimental setup and measurement techniques used. Section 4 presents the experimental data and interpretation. The conclusions are drawn in Section 5.

2. Theoretical Framework

The idea behind the present method is to combine an interferometric technique for measuring ultra-small displacements with the thermal sensitivity of the shape of a thermostatic bimetallic strip (BS). A "bimetal" may be manufactured by bonding together two strips having different thicknesses, made of different metals or alloys [15]. It is commonly noted that different alloys have different thermal expansion properties. Figure 1(a) schematically shows a BS made of strips (1) and (2) of different metals. They have the same length l_0 in some particular state [A] with temperature T_0 (where the BS is flat). When heated to another state [B] with temperature $T > T_0$, strip (1) elongates more than strip (2) if the linear thermal expansion coefficients of the two metals satisfy the condition $\beta_1 > \beta_2$. Because strips (1) and (2) are permanently joined, a contact interaction develops between the metals and causes the BS to take an arc shape. Heating-induced bending increases as the temperature increases and reverses when the temperature decreases. If $T < T_0$, the BS will bend in the opposite direction because the two metals will also contract at different rates. Strip (1), which develops a larger thermal expansion, is called the active layer, whereas strip (2), with lower expansion, is known as the passive layer. The active components often consist of Ni, Fe, Mn, or Cr alloys of various compositions. The passive component is, in general, the Invar alloy Fe-Ni with 36% Ni. Some BSs with high electrical and thermal conductivities have a third layer of Cu or Ni "sandwiched" between the active and passive layers.

The curvature C of a BS subjected to temperature variation is given by the Timoshenko-Ehrenfest theory [16] as a function of the thicknesses d_1, d_2 of

the component alloys, their respective Young's moduli E_1, E_2, and the difference $T - T_0$ between the current and reference temperatures. For $d_1 = d_2$, the expression in Ref. [16] can be simplified to

$$C = k\left(T - T_0\right)/d\,, \tag{1}$$

where d is the total thickness of the BS and the constant $k = 24E_1E_2\left(\beta_1 - \beta_2\right)/\left(E_1^{\,2} + 14E_1E_2 + E_2^{\,2}\right)$ is characteristic of the pair of alloys and is known as the "specific curvature" or "flexivity" [15]. Therefore, the specific curvature can be defined as the change in BS curvature per unit temperature change multiplied by the thickness, in the absence of external forces.

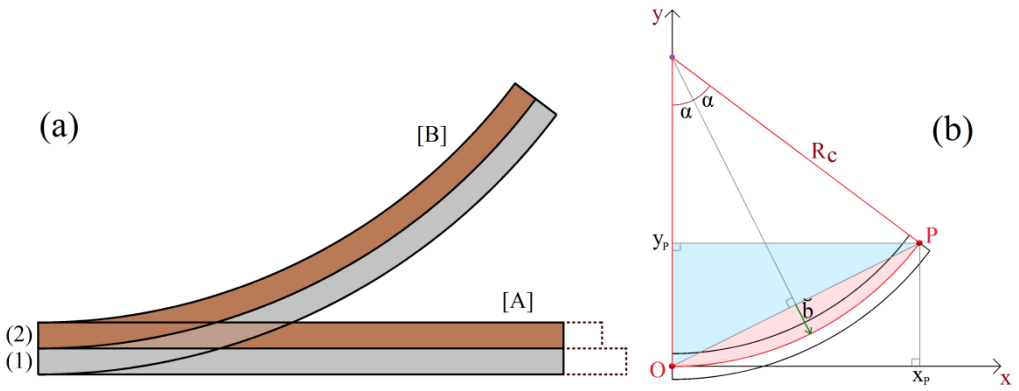

Fig. 1. (a) The two bonded strips (1) and (2) have the same length at the reference temperature in [A]. When heated to a higher temperature, the metals expand differently, and the BS is forced to bend as shown in [B]; (b) Geometry of the thermostatic BS deflection.

Figure 1(b) shows the heated BS in the *x*-*y* Cartesian plane. We denote the axis of the unbend strip at the reference temperature by *x* and we consider that the BS is fixed at point *O* so that it remains tangent to the *x* axis regardless of the temperature variations. The coordinates x_P and y_P of the free-end *P* of the BS may be related to its curvature radius $R_c = 1/C$ by observing that $\sin(2\alpha) = x_P / R_c$, $\cos(2\alpha) = 1 - y_P / R_c$, and $\alpha = l/(2R_c)$, where 2α is the total angular deflection and l is the median arc length of the strip at the current temperature T. Therefore, we have

$$x_P = \sin(lC)/C\,; \tag{2x}$$

$$y_P = \left[1 - \cos(lC)\right]/C\,. \tag{2y}$$

The coordinates x_P and y_P are related by the Cartesian equation

$$x_P^{\,2} + \left(y_P - R_c\right)^2 = R_c^{\,2}\,. \tag{3}$$

The strip middle deflection $\breve{b}$ (Fig. 1(b)) can be written as a function of temperature. Because $\breve{b} = R_c\left[1-\cos(\alpha)\right] = 2R_c \sin^2(\alpha/2)$ and $2\alpha = l/R_c = lC$, using Eq. (1), $\breve{b}$ can be expressed as

$$\breve{b} = \frac{2d\sin^2\left[\dfrac{lk(T-T_0)}{4d}\right]}{k(T-T_0)} = \operatorname{sinc}^2\left[\beta(T-T_0)\right]\beta(T-T_0)\frac{l}{2}, \tag{4}$$

where $\beta = lk/(4d)$ is a constant specific to the BS. Since for small temperature variations we have $\beta(T-T_0) << 1$ and $\operatorname{sinc}^2\left[\beta(T-T_0)\right] \cong 1$, Eq. (4) can be approximated by the linear expression

$$\breve{b} \cong \beta(T-T_0)\frac{l}{2}. \tag{5a}$$

If the temperature gradient of the BS is non-zero, it can be verified easily (see the Appendix) that approximation in Eq. (5a) is still valid in the form

$$\breve{b} \cong \beta(\overline{T}-T_0)\frac{l}{2}, \tag{5b}$$

where $\overline{T} = \frac{1}{l}\int_0^l T(x)dx$ is the spatial average temperature of the BS.

Let us assume that the movable mirror of a Michelson-type interferometer is attached to the middle point of the BS. If the deflection $\breve{b}$ is parallel to the laser beam and changes with time τ, the variation of the phase difference between the interfering laser waves is [17]

$$\delta\varphi(\tau) = 4\pi\breve{b}(\tau)/\lambda, \tag{6}$$

where λ denotes the laser wavelength. The phase variation determines a shift in the interference pattern at the detector, such as

$$N(\tau) = \delta\varphi(\tau)/2\pi = 2\breve{b}(\tau)/\lambda, \tag{7}$$

where N is the number of fringes that "sweep" the detector in time τ. Thus, the number of fringes that pass through the detector can be used to deduce the middle deflection of the BS as a function of time, that is

$$\breve{b}(\tau) = N(\tau)\lambda/2. \tag{8}$$

Using Eqs. (5b) and (8), the dependence on time of the BS average temperature variation $\Delta T(\tau) = \overline{T}(\tau) - T_0$ can be expressed as

$$\Delta T(\tau) \cong \frac{N(\tau)\lambda}{\beta l}. \tag{9}$$

3. Experimental setup and technique

Chase E-120 thermostatic BS, which is a high-expansion Mn-Cu-Ni alloy with a thickness of $d = 0.15\,\text{mm}$, protected by a thin layer of Ni-Cr steel, was used. This reliable bimetal has some built-in advantages: high flexivity, high thermal conductivity, and corrosion resistance. In a first stage, we measured the specific thermal curvature of the BS in a water bath at a controlled temperature. It is a simple but very effective method, for two reasons: (i) the thermal inertia of water allows a quasi-static heating process and (ii) the slow water heating guarantees the temperature uniformity of the submerged BS. In a second stage, the interferometry measurements were carried out.

The BS was fixed by its support such that its width was vertical and the strip was not in contact with the bottom of the tray, as shown in Fig. 2(a). The length of the moving part of the strip was determined as $l = 109\,\text{mm}$. As the temperature of the BS changes, it is deflected such that it forms an arc of a circle with variable curvature, as described in Section 2. The BS was fixed on the support at point *O* such that at the reference temperature it was oriented along one of the thick lines of a paper grid (denoted by *x*-axis) (Fig. 2(b)). The coordinates x_P and y_P of the BS free-end *P* depend on the water temperature.

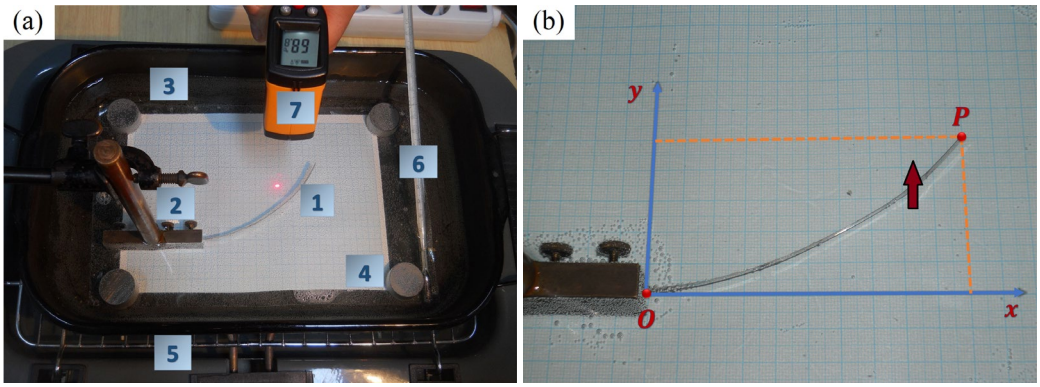

Fig. 2. (a) Experimental setup used to measure the BS thermal specific curvature: (1) bimetal strip; (2) vertical support; (3) metallic tray with water; (4) plastic laminated sheet of millimetric paper; (5) electric heat source; (6) mercury thermometer; (7) infrared thermometer; (b) positioning details of the deflected BS in warm water.

The water was initially cooled down close to the freezing point (y_P became negative), and then warmed up using an electrical heat source (y_P changed to positive values). The temperature was slowly varied between 2°C and 95°C. The position of the free end of the BS was recorded at multiple temperature points. The submerged mercury thermometer has an accuracy of $0.5\,\text{K}$, but exhibits a relatively higher thermal inertia. We also used a non-contact infrared

thermometer (Benetech GM320) that was cross-checked with the classical thermometer to exclude aberrant readings. The infrared thermometer displays the water surface temperature in $\sim 0.8\,\mathrm{s}$ but it only has an accuracy of $2\,\mathrm{K}$. The x_P and y_P coordinates were measured with millimeter accuracy.

We used a highly stable laser interferometer mounted on a heavy optical table with double protection against mechanical vibrations (low-frequency mechanical dumping at the base and air-chamber pneumatic suspensions under the table top plate). Figure 3 schematically shows the top view of the experimental interference setup.

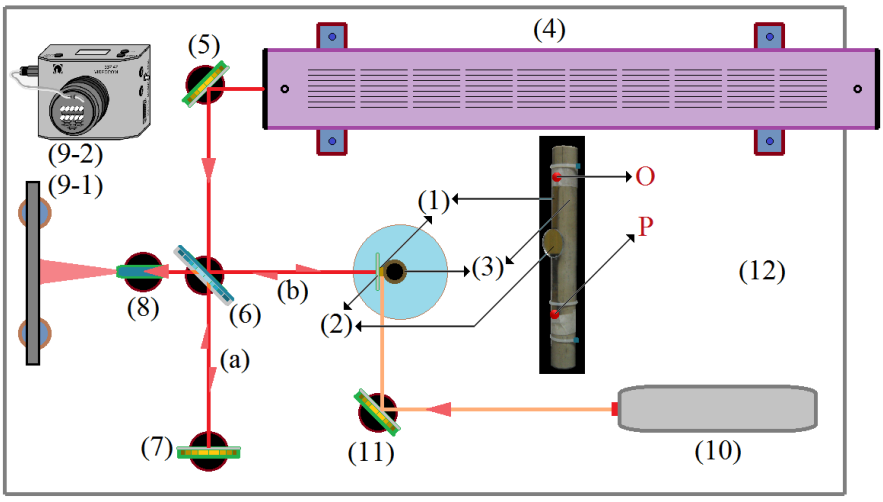

Fig. 3. The experimental interferometry setup: (1) Mn-Cu-Ni thermostatic BS; (2) small circular mirror; (3) cylindrical ceramic support; (4) HNA188 Carl Zeiss He-Ne laser source; (5) adjustable mirror; (6) continuously variable beam splitter VBA-200; (7) adjustable mirror tilter MH-50; (8) microscope objective $40^{X}0.65$; (9-1) white observation screen; (9-2) VIDEOCOM CCD camera; (10) auxiliary He-Ne laser source; (11) adjustable mirror; (12) optical table top plate. The inset shows the picture of the BS-mirror mounting on the ceramic support.

The primary $20\,\mathrm{mW}$ beam of the He-Ne laser (4) ($\lambda = 632.8\,\mathrm{nm}$) is aimed at mirror (5) and then separated by a variable transparency beam splitter (6) into two secondary laser beams (a) and (b). In our setup, the optical paths of the secondary beams are almost equal. One of them (a) is reflected back by an adjustable mirror (7), whereas the other (b) is reflected by a small mirror (2) glued in the middle of the BS (1) on a tiny central spot. Thus, the small mirror is expected to have micrometer displacements along the beam (b) when the BS is heated or cooled during the experiment. The BS was fixed at one end (point *O* in the inset) to the upper part of a ceramic tube (3), by immobilizing a small portion of it, equal to the one used to hold it in the water bath. The BS was parallel to the ceramic tube, which was mounted vertically on a rigid support. The other end

(point *P* in the inset) was not rigidly fixed to the lower part of the ceramic tube, but only prevented from losing contact with it, with the help of a loose plastic tie. This minimizes the oscillations of the BS-mirror system as a gravitational pendulum and avoids any additional longitudinal tension during heating/cooling cycles. Thus, the BS can be slightly curved and the displacements of the mirror (2) correspond to the middle deflection of the BS. We considered that the own mass of the small mirror doesn't have an influence on the lateral curvature of the BS, given that the strip is mounted vertically and its middle lateral deflection is micrometric. When heated, the concave part of the BS was oriented toward the ceramic tube, and the distance between the small mirror and the tube increased. The reflected secondary beams (a) and (b) were recombined through the splitter and propagated through the microscope objective (8) as a single tertiary beam. This beam was expanded by the objective and visualized on the white screen (9-1) as a large circular interference pattern. We have used as an optical heating source the beam of a second He-Ne laser (10) ($\lambda = 632.8\,\text{nm}$) with an output power of $5\,\text{mW}$. This auxiliary laser beam is aimed at mirror (11) on the middle BS, where, because the BS has a large reflectivity, only a small part of the laser energy is absorbed. However, the BS expands as a result of this ultra-small temperature change and its displacement causes a measurable motion of the interference pattern on the screen. The slowly changing pattern can be directly observed on the white screen (9-1) or captured using a CCD camera (9-2) as a detector. The screen, which is mostly used for optical adjustments of the interference setup, was replaced for measuring purposes with the CCD camera connected to a computer. The CASSY-Lab software was used to analyze the moving interference pattern and count the number of displaced fringes.

4. Results and discussion

4.1. *Bimetal specific curvature and thermal deflection rate*

Figure 4 shows the dependence of the BS free-end *P* position on temperature. The measured values and interpolation theoretical curves were plotted. Because the precision of the position reading is $0.5\,\text{mm}$, vertical error bars are not displayed. The horizontal error bars represent the precision of the infrared thermometer. Figures 4(a) and 4(b) present the measured coordinates of the strip free-end and the theoretical fit of the experimental points using Eqs. (2x) and (2y). We found the value $k = 33.6 \cdot 10^{-6}\ \text{K}^{-1}$ of the specific curvature, using a nonlinear regression fitting algorithm.

In Fig. 5(a), we show the position of point *P* in the *x*-*y* plane at the same temperature values as in Fig. 4. The experimental points were fitted with the theoretical curve given by Eq. (3) and using the previously estimated value of the specific curvature. On the left-side vertical axis in Fig. 5(b), we show the

curvature radius of the BS as a function of temperature, calculated using Eq. (1) and the estimated value of k. On the right axis, the deflection given by Eq. (4) is presented as a function of temperature. Negative values of R_c and $\breve{b}$ correspond to the bending of the BS such as y_P was negative. Optical measurements were performed at room temperature ($t = 23\,°C$).

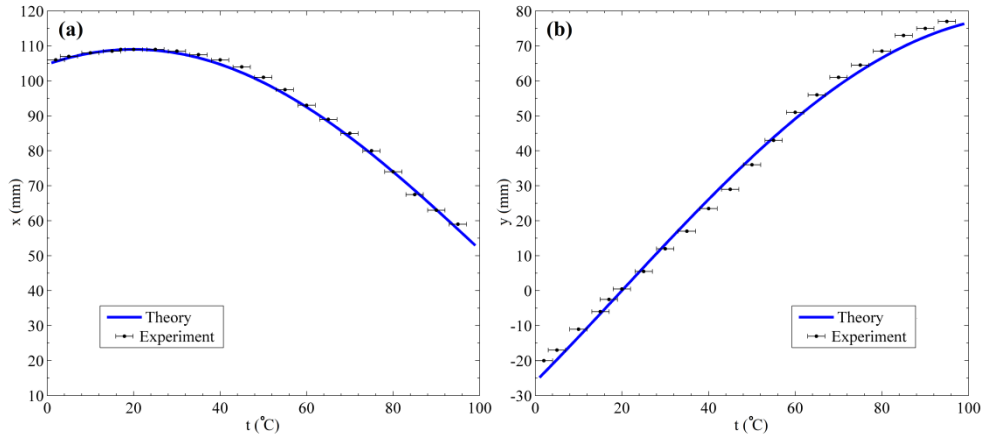

Fig. 4. Dependence on the temperature of the (a) *x*-coordinate; (b) *y*-coordinate of the free-end *P* of the BS.

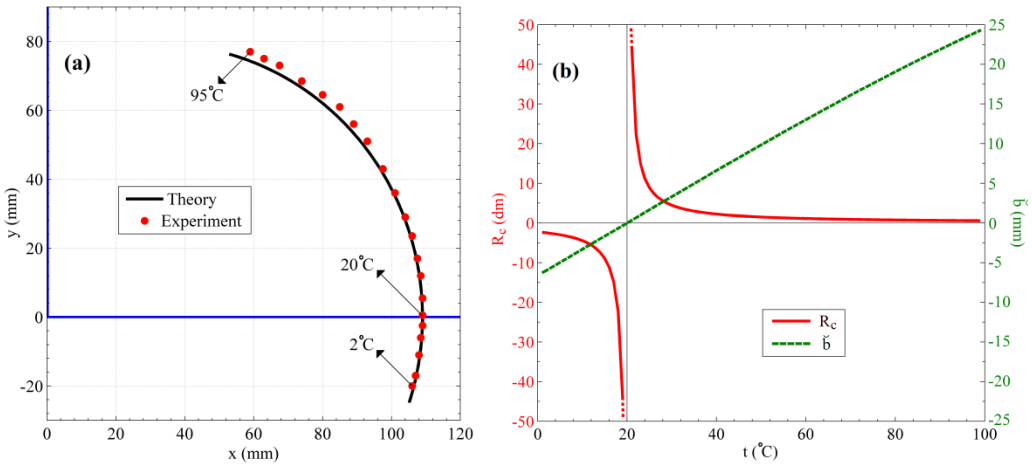

Fig. 5. (a) Position in the *x*-*y* plane of the free-end *P* of the BS; (b) Curvature radius and deflection of the bimetal strip as functions of temperature.

The slight disagreement between the experimental and theoretical curves in Figs. 4(b) and 5(a) is likely induced by the deviation of a real BS from the ideal theoretical model. It is about Timoshenko's assumption that, under ideal conditions, the difference between the coefficients of thermal expansion of the

metals that form the BS remains constant with the temperature variation [16]. In practice this can only be approximately true, which can lead to small deviations from the linearity with temperature expressed by Eq. (1). However, the disagreement is only observed at higher temperatures.

Because the deflection $\breve{b}$ versus temperature t function in Fig. 5(b) is not perfectly linear (Eq. (5a) holds only for small variations), we may expect a non-constant rate of variation $d\breve{b}/dT$. We present this quantity in Fig. 6 as a function of temperature. As shown in the inset, at room temperature, the estimated value of $d\breve{b}/dT$ was 332.5 µm/K. Because of the interferometric setup, strip deflections can be measured in the order of $\lambda/2 \approx 0.316$ µm, making it clear that detecting temperature variations within the precision $\lambda/2 \cdot \left(\mathrm{d}\breve{b}/\mathrm{dT}\right)^{-1} \approx 1$ mK is feasible. The use of green or blue lasers may further improve the accuracy of this method, benefiting from a shorter wavelength.

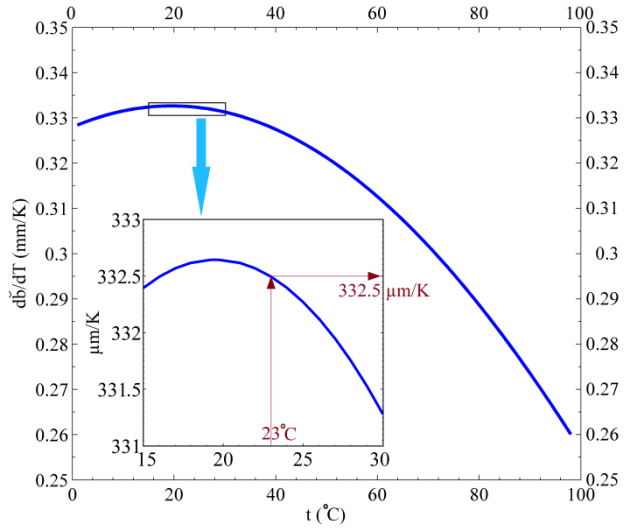

Fig. 6. Rate of deflection variation versus the temperature. The inset zooms in the vicinity of the room temperature point.

4.2. *mK variations of the bimetal temperature*

The optical setup presented in Fig. 3 is useful for investigating the thermal processes with extremely small temperature variations. To prove this, we measured the displacement of the interference pattern generated during free cooling of the BS. First, the interference pattern was observed by reflection on the white screen (9-1) mounted in place of the CCD camera (9-2). Figure 7 shows a sequence of photo images captured in the dark which correspond to consecutive displacements of approximately $\lambda/8$ of the small mirror (2), at slightly different temperatures of the BS.

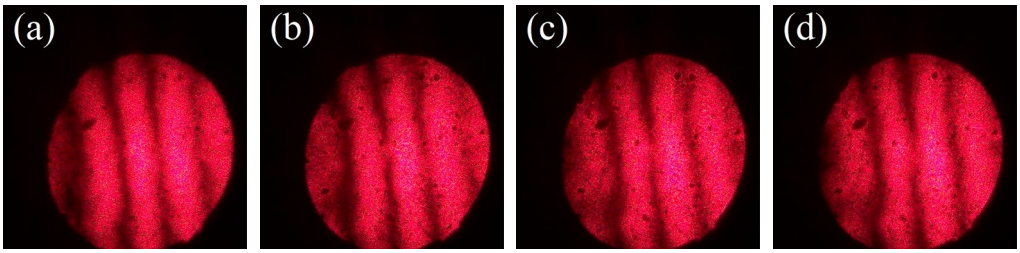

Fig. 7. Interference patterns at successive slightly different temperatures, for which the middle deflection of the BS changes with one eighth of the wavelength from one image to another.

The CCD measurements were performed after a time of continuous heating of the BS by the auxiliary He-Ne laser beam. The acquisition session had been started $\sim 100\,\mathrm{s}$ before the laser was switched off. This delay was used to confirm that quasi-steady fringes were observed before the heating was stopped. Because the laser beam irradiates the BS on a small central area, it is expected that the temperature will not be constant along the bimetal when the laser is turned off. That is why, during cooling, we will take into account the evolution over time of the spatial average temperature $\overline{T}$ of the BS. In Fig. 8(a), we see that at $\tau = 101\,\mathrm{s}$ the heating source was switched off and the strip began to cool down. The deflection decreased, and the interference pattern started to "sweep" the objective of the CCD camera. The software "looks" for the movement of the fringes by recording the position of the most photo-excited pixel in the array of 2048 photoelements of the CCD at every moment. The software-allowed time reading precision was $100\,\mathrm{ms}$. For a total measurement time of $25\,\mathrm{s}$, the software detected 23 bright fringes that swept the camera objective. Noticeably, Fig. 8(a) contains information about function $N(\tau)$, that is, the dependence of the number of fringes N on the time τ. This can be understood as a discrete function of time, if we consider the series of moments at which the middle of each bright fringe is recorded.

Using values $l = 109 \cdot 10^{-3}\,\mathrm{m}$, $d = 150 \cdot 10^{-6}\,\mathrm{m}$, and $k = 33.6 \cdot 10^{-6}\,\mathrm{K}^{-1}$ (from previous experiment), we obtain $\beta \cong 6.1 \cdot 10^{-3}\,\mathrm{K}^{-1}$. In addition, because we expect temperature variations of the order of tens of mK, we have $\beta(\overline{T} - T_0) \approx 10^{-4}$. Therefore, the approximation given by Eq. (5b) is completely justified. The dependence of the BS average temperature variation ΔT on time τ can be numerically calculated using Eq. (9) and the discrete function $N(\tau)$ inferred from Fig. 8(a). The function $\Delta T(\tau)$ was plotted in Fig. 8(b) as a discrete set of points. The interpolation was performed to visualize a continuous variation. A total temperature drop of approximately $22\,\mathrm{mK}$ is observed. As expected, the variation is non-linear, faster at the beginning and slower afterwards.

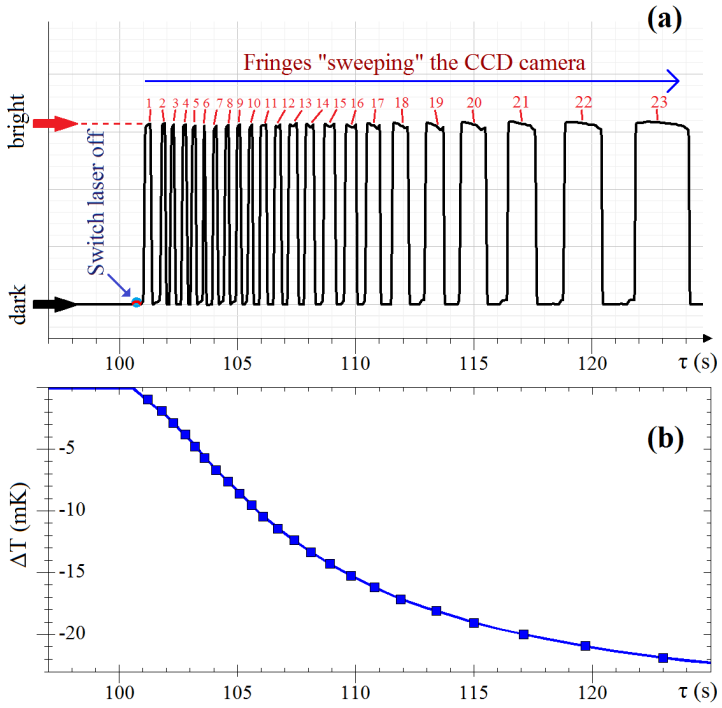

Fig. 8. (a) Plot generated by the acquisition software: fringe detection versus time. Raw image has been processed to increase quality and add some graphical information. (b) Average temperature variation of the BS as a function of time. Each blue square corresponds to a fringe in Fig. (a).

We provided evidence that milliKelvin sensitivity could be achieved. The principle could be replicated in a mini-device and used as an ultra-sensitive temperature detector after rigorous absolute calibration.

5. Conclusions

Ultra-sensitive temperature measurements are difficult to obtain and special techniques must be employed to accomplish this task. In this study, we proposed a simple method for measuring ultra-small temperature variations. Our method combines laser interferometry and dilatation of a bimetallic strip to build a temperature sensor. We proved that temperature variation measurements with milliKelvin sensitivity are feasible. Further improvements are possible by using smaller-wavelength lasers and miniaturizing the design.

REFERENCES

[1] *T. D. McGee*, Principles and methods of temperature measurement, John Wiley & Sons, New York, 1988.
[2] *P. R. N. Childs, J. R. Greenwood, C. A. Long*, Review of temperature measurement, *Rev. Sci. Instrum.* 71 (8), 2959–2978 (2000).
[3] *C. W. Meyer* (ed.), Temperature: its measurement and control in science and industry, Vol. 8, Proceedings of the 9th International Temperature Symposium 1552 (1), 2012.

[4] *J. G. Webster (ed.), H. Eren* (ed.), Measurement, instrumentation, and sensors handbook: spatial, mechanical, thermal, and radiation measurement, 2nd edition, CRC Press, Taylor & Francis Group, Boca Raton, 2014.
[5] *H. W. Yoon, V. Khromchenko, G. P. Eppeldauer,* Improvements in the design of thermal-infrared radiation thermometers and sensors, Optics Express 27 (10), 14246–14259 (2019).
[6] *F. Pompei, M. Pompei*, Non-invasive temporal artery thermometry: Physics, Physiology, and Clinical Accuracy, Proceedings of the SPIE 5405, 2004.
[7] *H. Preston-Thomas*, The International Temperature Scale of 1990 (ITS-90), Metrologia 27, 3–10 (1990).
[8] *H. M. Hashemian, K. M. Petersen*, Achievable Accuracy and Stability of Industrial RTDs, Temperature: its measurement and control in science and industry, Vol. 6, 427–431 (1992).
[9] *H. H. Volker*, High-precision measurement of absolute temperatures using thermistors, Proc. Estonian Acad. Sci. Eng. 13 (4), 379–383 (2007).
[10] *D. R. White, R. Galleano, A. Actis, H. Brixy, M. De Groot, J. Dubbeldam, A. L. Reesink, F. Edler, H. Sakkurai, R. L. Shepard, J. C. Gallop,* The status of Johnson noise thermometry, Metrologica 33, 325–335 (1996).
[11] *S. Menkel, D. Drung, C. Assmann, T. A. Schurig*, A Resistive dc SQUID Noise Thermometer, Appl. Supercond. 6, 417–422 (1998).
[12] *C. P. Lusher, J. Li, V. A. Maidanov, M. E. Digby, H. Dyball, A. Casey, J. Nyeki, V. V. Dmitriev, B. P. Cowan, J. Saunders,* Current sensing noise thermometer using a low TC DC SQUID preamplifier, Meas. Sci. Technol. 12, 1–15 (2001).
[13] *J. Beyer, D. Drung, A. Kirste, J. Engert, A. Netsch, A. Fleischmann, C. Enss*, A magnetic-field-fluctuation thermometer for the mK range based on SQUID-magnetometry, IEEE Transactions on Applied Superconductivity 17 (2), 760–763 (2007).
[14] *T. C. Cetas*, A Magnetic Temperature Scale from 1 to 83 K, Metrologia 12, 27–40 (1976).
[15*] Kanthal AB, Kanthal* Thermostatic Bimetal Handbook, 6th edition, Hallstahammar, Sweden, 2008.
[16] *S. P. Timoshenko*, Analysis of bi-metal thermostats, J. Opt. Soc. Am. 11, 233 (1925).
[17] *F. L. Pedrotti, L. M. Pedrotti, L. S. Pedrotti*, Introduction to Optics, 3rd edition, Cambridge University Press, Cambridge, 2017.

Appendix

The shape of a BS with variable temperature deviates from a circular arc. We denote by $u(x)$ the angle made by the BS with x axis, so that $u(0)=0$ and $u(x_P)=2\alpha$. The BS contained between x and $x+dx$ can be considered as an infinitesimal circular arc with temperature $T(x)$, curvature $C(x)$, and angle

$$du = u(x+dx)-u(x) = C(x)dx = k\frac{T(x)-T_0}{d}dx. \tag{A1}$$

In the approximation of small deflections we integrate Eq. (A1) between 0 and $x_P \cong l$ and we obtain the total angular deflection

$$2\alpha \cong \frac{lk}{d}\left[\frac{1}{l}\int_0^l T(x)dx - T_0\right] = 4\beta\left(\overline{T}-T_0\right). \tag{A2}$$

Using Eq. (A2), the middle BS deflection can be approximated as

$$\breve{b} \cong \frac{\alpha l}{4} = \frac{l^2 k}{8d}\left(\overline{T}-T_0\right) = \beta\left(\overline{T}-T_0\right)\frac{l}{2}. \tag{A3}$$

Notice that $\breve{b}$ is a linear function of $\overline{T}$ and a quadratic function of l.